

Evolution of Close Neutron Star Binaries

Wataru Ogawaguchi¹ and Yasufumi Kojima²

¹ Department of Physics, Tokyo Metropolitan University
Hachioji, Tokyo, 192-03 JAPAN

² Department of Physics, Hiroshima University
Higashi-Hiroshima, Hiroshima, 739 JAPAN

July 27, 2021

Abstract

We have calculated evolution of neutron star binaries towards the coalescence driven by gravitational radiation. The hydrodynamical effects as well as the general relativistic effects are important in the final phase. All corrections up to post^{2.5}-Newtonian order and the tidal effect are included in the orbital motion. The star is approximated by a simple Newtonian stellar model called affine star model. Stellar spins and angular momentum are assumed to be aligned. We have showed how the internal stellar structure affects the stellar deformation, variations of the spins, and the orbital motion of the binary just before the contact. The gravitational wave forms from the last a few revolutions significantly depend on the stellar structure.

1 Introduction

Direct detection of gravitational waves will be possible in not so far future by the recent constructing laser interferometers such as LIGO [1]. One of the promising sources is coalescing compact star binary consisting of neutron stars or black holes. The coalescence rate of the binary is estimated as $\sim 10^{-7}\text{yr}^{-1}\text{Mpc}^{-3}$ [2, 3]. If we can observe up to a few hundred Mpc, we have a few events by a year. The detection of the gravitational wave is not only an important probe of general relativity, but also a new tool of measurement of Hubble constant and high density nuclear matter [4, 5].

Theoretically, it is important to understand the final phase of the binary coalescence, that is, how the binary evolves from the separation distance of a few hundred km to the contact or disruption of the binary. The frequency of the gravitational radiation at this phase corresponds to the observational frequency band, about $10 \sim 10^3$ Hz. The preparation of the gravitational wave form as the template is necessary for the matched filter analysis. When the separation L of the binary is much larger than the stellar radius R , each star can be regarded as a point mass. The study to get the matched filter is currently in progress using the higher order post-Newtonian approximation [6, 7]. In particular, the test particle limit is extensively studied by the perturbation of the black hole space-time. (See e.g., Ref. [8, 9].) The rotational velocity gradually increases with shrinking of the orbital radius, and therefore higher post-Newtonian corrections become crucial. When L is a few times R , hydrodynamical effects also become important. The only method to examine the final stage may be solving the Einstein equations numerically. Available memory and speed of the computers are limited at present, so that the simulations are carried out with the Newtonian or post-Newtonian approximation, or preliminary results are obtained in fully relativistic case. (See Ref.[10, 11] and therein.)

One of hydrodynamical effects before the contact of the binary is tidal force. Lai, Rasio & Shapiro calculated the dynamical evolution of the binary of simplified stellar models under the Newtonian gravity [12, 13, 14]. They showed that the orbit significantly deviates from that of two point masses. The reason is that there is additional contribution from the stellar quadrupole moment, which causes marginally stable circular orbit at $L = (2 \sim 3)R$. When the separation becomes below the critical distance, the radial infall velocity significantly accelerates in addition to the radiation reaction force. However, since the tidal potential depends on L^{-6} , the effect is significant only for close binary, i.e., higher post-Newtonian correction. Natural question is whether the contribution is still significant, when other post-Newtonian corrections are included. The effect of the spinning star, i.e., spin-orbit and spin-spin interaction, may be important since the tidal torque changes the spin. They are respectively post^{1.5}-Newtonian and post²-Newtonian order in the magnitude. The first and second post-Newtonian corrections concerning the orbital motion are also important, when the tidal interaction becomes large. In this paper, we take all these corrections and the radiation reaction force into consideration, and study how the binary evolves at $L < 15R$. We adopt simplified stellar models called affine star models. The model is equivalent to the second order virial equation. In this approximation, the fluid displacement is limited to a certain class of the motion, i.e., uniform expansion, rotation and quadrupole oscillation. The dynamical degrees of

freedom of a star are reduced to finite number, and the equations of motion are not partial differential equations, but ordinary differential equations. Using this approximation, we can easily simulate the final phase of the binary with various effects concerning spin and quadrupole moment.

In §2, we present our model. We show the collection for the interactions up to the post²-Newtonian order and the radiation reaction force of post^{2.5}-Newtonian order. The affine star model is also briefly summarized. We show the deformation of the star, the orbital motion, the gravitational wave form and the evolution of the spin near the final stage just before the disruption of the binary in §3. In §4, we discuss the implication of our results.

2 Numerical Methods

2.1 Orbital motion

In order to solve orbital motion of the binary, we use the Hamiltonian formalism [15]. Regarding the star as a point mass with M_a ($a = 1, 2$), we will examine the relative orbital motion. The motion for the center of mass will not be considered here. The equations of motion can be described by the total mass M_T and reduced mass μ . We choose the orbital plane as the equatorial plane of the polar coordinate (r, θ, ϕ) . The Newtonian, the first and second post-Newtonian equations of motion are determined by the following Hamiltonians.

$$H_N = \frac{1}{2\mu} \left(p_r^2 + \frac{p_\phi^2}{r^2} \right) - \frac{G\mu M_T}{r}, \quad (1)$$

$$H_{PN} = \frac{3\nu - 1}{8c^2\mu^3} \left(p_r^2 + \frac{p_\phi^2}{r^2} \right)^2 - \frac{GM_T}{2c^2\mu r} \left\{ (3 + \nu) \left(p_r^2 + \frac{p_\phi^2}{r^2} \right) + \nu p_r^2 \right\} + \frac{G^2\mu M_T^2}{2c^2r^2}, \quad (2)$$

$$\begin{aligned} H_{P^2N} = & \frac{1 - 5\nu + 5\nu^2}{16c^4\mu^5} \left(p_r^2 + \frac{p_\phi^2}{r^2} \right)^3 \\ & + \frac{GM_T}{8c^4\mu^3r} \left\{ (5 - 20\nu - 3\nu^2) \left(p_r^2 + \frac{p_\phi^2}{r^2} \right)^2 - 2\nu^2 p_r^2 \left(p_r^2 + \frac{p_\phi^2}{r^2} \right) - 3\nu^2 p_r^4 \right\} \\ & + \frac{G^2 M_T^2}{2c^4\mu r^2} \left\{ (5 + 8\nu) \left(p_r^2 + \frac{p_\phi^2}{r^2} \right) + 3\nu p_r^2 \right\} - \frac{G^3 (1 + 3\nu) \mu M_T^3}{4c^4 r^3}, \end{aligned} \quad (3)$$

where $\nu = \mu/M_T$.

Next, we consider the effect of the quadrupole moment of a star. If the star has mass quadrupole moment, the Newtonian gravitational potential has an additional contribution, $\sim 1/r^3$. The relative motion is affected by the monopole-quadrupole interaction [16],

$$H_T = -\frac{G}{2r^3} \left(3n^i n^j - \delta^{ij} \right) \left\{ M_2 (\mathbf{I}_1)_{ij} + M_1 (\mathbf{I}_2)_{ij} \right\}, \quad (4)$$

where $\mathbf{n} = \mathbf{r}/r$ and \mathbf{I}_a is mass quadrupole moment of star a ($a = 1, 2$).

The spin-orbit and spin-spin interaction term in appropriate coordinate system can be written as [16],

$$H_{SO} = \frac{G}{c^2 r^3} \mathbf{L}_N \cdot \left\{ \left(2 + \frac{3M_2}{2M_1} \right) \mathbf{J}_1 + \left(2 + \frac{3M_1}{2M_2} \right) \mathbf{J}_2 \right\}, \quad (5)$$

$$H_{SS} = \frac{G}{c^2 r^3} \{ 3(\mathbf{J}_1 \cdot \mathbf{n})(\mathbf{J}_2 \cdot \mathbf{n}) - (\mathbf{J}_1 \cdot \mathbf{J}_2) \}, \quad (6)$$

where \mathbf{J}_a is spin angular momentum of star a and \mathbf{L}_N is orbital angular momentum of the Newtonian order, i.e., $\mathbf{L}_N = \mathbf{r} \times \mathbf{p}$.

Now, we shall estimate the order of magnitude for these various forces here. Suppose that a binary system consists of compact stars with mass $M_a \sim M$ and radius $R_a \sim R$ ($a = 1, 2$). The orbital velocity v at the separation distance L is $v \sim (GM/L)^{1/2}$. We define the dimensionless relativistic factor, ϵ as $\epsilon = (GM/Lc^2) \sim (v/c)^2$. Since the radius of the compact star is of order GM/c^2 , the spin angular momentum J and the quadrupole moment I can be written as $J = \alpha GM^2/c$ and $I = \beta G^2 M^3/c^4$, where α and β are dimensionless numbers. The maximumly rotating Kerr black hole corresponds to $\alpha = 1$. It is likely that $\alpha < 1$. The value of β is small in isolated system, but is induced by the companion star as $\beta \propto (R/L)^3 \sim \epsilon^3$.

We shall write the Newtonian force as $f_N = GM^2/L^2$, which can be estimated as $\partial H_N/\partial r \sim H_N/L$. The order of the first and second post-Newtonian corrections are ϵf_N and $\epsilon^2 f_N$, respectively. The tidal interaction is the Newtonian force, but the magnitude for the compact star is $GIM/L^4 \sim \beta \epsilon^2 f_N \sim \epsilon^5 f_N$. This is higher post-Newtonian correction. The spin-orbit coupling term is formally the post-Newtonian correction, since the term contains the factor G/c^2 . The magnitude is, however, estimated as $G/c^2 \times MLv \times J/L^4 \sim \alpha \epsilon^{3/2} f_N$, that is, the spin-orbit force is the post^{1.5}-Newtonian correction practically. In the similar way, the spin-spin interaction is also formally the post-Newtonian correction, but practically the post²-Newtonian correction as $G/c^2 \times J^2/L^4 \sim \alpha^2 \epsilon^2 f_N$. The equations of motion can be determined by the sum of these Hamiltonians.

2.2 Affine star model

As seen in the previous section, the orbital motion is affected by the spin angular momentum J_i and the mass quadrupole moment I_{ij} , as well as the mass M . The spin and the quadrupole moment are determined by the stellar structure. We adopted so-called the affine star model for the stellar model. In this section, we will summarize the single affine star model [17, 18]. The binary consists of two affine star models ($a = 1, 2$). In this section, we omit the suffix a and use the Cartesian coordinate system, whose origin is the mass center of a single star.

The position of a fluid element inside the star, $x_i(t)$ is specified by the Lagrangian map from its initial position \hat{x}_i as

$$x_i(t) = q_{ia}(t) \hat{x}_a, \quad (7)$$

where q_{ia} is 3×3 matrix and $q_{ia}(0) = \delta_{ia}$. The initial sphere of radius R is transformed into an ellipsoid as

$$S_{ij}^{-1}x_ix_j = R^2, \quad (8)$$

where S_{ij}^{-1} is the inverse of a symmetric matrix, $S_{ij} = q_{ia}q_{ja}$. The eigenvalues of S_{ij} determine three principal axes of the ellipsoid.

The dynamics of the fluid motion can be determined in the Hamiltonian formalism by the generalized coordinate q_{ia} and its conjugate momentum $p_{ia} = I_0\dot{q}_{ia}$, where the inertial moment I_0 is described $I_0 = \frac{1}{3} \int \hat{x}_a\hat{x}_a dM$ and the dot denotes time derivative. The initial state is a spherically symmetric star with mass M and radius R , and we assume a polytropic equation of state. So that we have $I_0 = \frac{1}{5}\kappa_n MR^2$, where κ_n is a constant relating with polytropic index n . The Hamiltonian concerning the internal fluid motion is the sum of the kinetic energy T , internal energy U , and self-gravitational energy Φ ,

$$H_I = T + U + \Phi. \quad (9)$$

The kinetic energy is a function of p_{ia} given by

$$T = \frac{1}{2} \int v_iv_idM = \frac{1}{2I_0} p_{ia}p_{ia}. \quad (10)$$

The internal energy is a function of q_{ia} . We use a polytropic equation of state, $P = \kappa\rho^{1+(1/n)}$, then the internal energy of the star is

$$U = \int \frac{nP}{\rho} dM = U_0 |\mathbf{q}|^{-1/n}, \quad (11)$$

where $|\mathbf{q}|$ is determinant of q_{ia} , and U_0 is the initial internal energy. The self-gravitational energy of the star can be calculated by an elliptical integral [19]

$$\Phi = \frac{1}{2} \Phi_0 S_{ik} \int_0^\infty \frac{(\mathbf{S} + u\delta)_{ik}^{-1}}{|\mathbf{S} + u\delta|^{\frac{1}{2}}} du, \quad (12)$$

where Φ_0 is the self-gravitational energy of spherically symmetric star. Since the pressure force and self-gravity assumed to balance at the initial state, we have

$$U_0 = -\frac{\Phi_0}{3} = \frac{GM^2}{(5-n)R}. \quad (13)$$

The quadrupole moment and the spin of the affine star model are given by

$$I_{ij} = I_0 q_{ia} q_{ja}, \quad (14)$$

$$J_i = \varepsilon_{ijk} q_{ja} p_{ka}. \quad (15)$$

2.3 Equations of motion and gravitational radiation

The dynamical degrees of freedom of the system are reduced to finite number in our approximation. The variables are fluid ones (q_{ij}, p_{ij}) and orbital ones (r, ϕ, p_r, p_ϕ) . The system is determined by the following total Hamiltonian,

$$H = H_{I1} + H_{I2} + H_N + H_{PN} + H_{P^2N} + H_T + H_{SO} + H_{SS}. \quad (16)$$

The evolution of \mathbf{J}_a ($a = 1, 2$) is governed by the familiar formula [16],

$$\begin{aligned} \frac{d\mathbf{J}_a}{dt} = & \frac{G}{c^2 r^3} \left\{ \left(2 + \frac{3M_b}{2M_a} \right) \mathbf{L}_N - \mathbf{J}_b + 3(\mathbf{n} \cdot \mathbf{J}_b) \mathbf{n} \right\} \times \mathbf{J}_a \\ & - \frac{3GM_b}{r^3} (\mathbf{n} \times (\mathbf{I}_a : \mathbf{n})), \end{aligned} \quad (17)$$

where the subscript b means that $b = 2$ for $a = 1$, and $b = 1$ for $a = 2$. The first term of eq.(17) represents the precession due to the spin-orbit and spin-spin coupling. This term changes the direction, but not the magnitude of the spin. Therefore, when the spins and angular momentum are aligned in the same direction, the first term vanishes and the direction of the spins is fixed. The second term shows that the magnitude of the spin changes through the tidal torque. It is easily checked that the above equation of spin is automatically satisfied, if (q_{ij}, p_{ij}) follow the equations of motion. Therefore, we do not have to calculate the evolution of spins additionally.

The system (16) is conserved one. We add the effect of the gravitational radiation by the lowest quadrupole formula, which is post^{2.5}-Newtonian order. The dissipative force is introduced by adding the radiation reaction forces $(f_r, f_\phi, F_r, F_\phi)$ in the Hamiltonian formalism (e.g., Ref.[20, 21]). The explicit radiation reaction forms are given by

$$f_r = -\frac{8G^2}{15c^5 \nu r^2} \left(2p_r^2 + \frac{6p_\phi^2}{r^2} \right), \quad (18)$$

$$f_\phi = -\frac{8G^2}{3c^5} \frac{p_r p_\phi}{\nu r^4}, \quad (19)$$

$$F_r = -\frac{8G^2}{3c^5} \frac{p_r}{r^4} \left(\frac{p_\phi^2}{\nu r} - \frac{G\nu M^3}{5} \right), \quad (20)$$

$$F_\phi = -\frac{8G^2}{5c^5} \frac{p_\phi}{\nu r^3} \left(\frac{2G\nu^2 M^3}{r} + \frac{2p_\phi^2}{r^2} - p_r^2 \right). \quad (21)$$

The evolution of the variables is determined by the following set of equations,

$$\frac{dr}{dt} = \frac{\partial H}{\partial p_r} + f_r, \quad (22)$$

$$\frac{d\phi}{dt} = \frac{\partial H}{\partial p_\phi} + f_\phi, \quad (23)$$

$$\frac{dp_r}{dt} = -\frac{\partial H}{\partial r} + F_r, \quad (24)$$

$$\frac{dp_\phi}{dt} = -\frac{\partial H}{\partial \phi} + F_\phi, \quad (25)$$

$$\frac{dq_{ij}}{dt} = \frac{\partial H}{\partial p_{ij}}, \quad (26)$$

$$\frac{dp_{ij}}{dt} = -\frac{\partial H}{\partial q_{ij}}. \quad (27)$$

We describe two polarization modes of gravitational waves by h_+ and h_\times . They are written by the distance to the source D and the directional angle Θ . Including the quadrupole moment terms of each ellipsoids, the polarization modes are given by,

$$h_+ = \frac{G}{2c^4 D} (1 + \cos^2 \Theta) \frac{d^2}{dt^2} \left[\mu r^2 \cos 2\phi + \sum_{a=1,2} \{(\mathbf{I}_a)_1 - (\mathbf{I}_a)_2\} \cos 2(\phi + \theta_a) \right], \quad (28)$$

$$h_\times = \frac{G}{2c^4 D} (2 \cos \Theta) \frac{d^2}{dt^2} \left[\mu r^2 \sin 2\phi + \sum_{a=1,2} \{(\mathbf{I}_a)_1 - (\mathbf{I}_a)_2\} \sin 2(\phi + \theta_a) \right], \quad (29)$$

where $(\mathbf{I}_a)_i$ ($i = 1, 2$) is the inertial moment of the ellipsoid along the principal axis a_i . Both a_1 and a_2 axes are chosen on the orbital plane of the binary. The a_1 axis is initially chosen as the separation direction \mathbf{n} of the binary and the a_2 axis is orthogonal to it. Three eigen-values of the matrix $(\mathbf{I}_a)_{ij}$ give $(\mathbf{I}_a)_i$ ($i = 1, 2, 3$). In eqs.(28), (29), θ_a is the lag angle, which is defined by the angle between the major axis of the ellipsoid a and the direction to the companion star. Tidally locked state corresponds to $\theta_a = 0$.

3 Results

We have calculated the evolution of close binary from a circular orbit of the separation $r = 15R$ to the contact, using two identical affine stars. The most natural orbit near $r = 15R$ is circular one, because the eccentricity is diminished by the gravitational radiation as the binary orbit shrinks. As for the internal structure at $r = 15R$, we adopt the equilibrium solution of the ellipsoid, i.e., irrotational Roche-Riemann ellipsoid or Maclaurin-Jacobi-Roche ellipsoid [22]. The former solution basically represents tidally locked, static figure in the inertial frame. We adopt Maclaurin-Jacobi-Roche solution as the spinning stellar model. Both stellar spins are assumed to be parallel to the orbital angular momentum, but the initial magnitude of spin is variable. The magnitude is parameterized by $\chi = |\mathbf{J}_a| / (\mathbf{I}_a)_3 \Omega_o$ at the initial separation, where Ω_o is the orbital angular frequency of the star. We selected the parameter as $\chi = -2, -1, -0.5, 0, 0.5, 1, 2$. The maximum rotation $|\chi| = 2$ in our model corresponds to the period of $\sim 40\pi t_D$, where t_D is the dynamical time at an individual star surface i.e., $t_D = (R^3/GM)^{1/2}$. Typically, it is about ten milliseconds for the actual neutron star. The results given below are almost

for $\chi = 0$ except in §3.3 and §3.4, because the results for $\chi \neq 0$ models are almost the same as those for $\chi = 0$. The stellar model is set up as $(GM/Rc^2) \simeq 0.2$ with polytropic index $n = 0.5$ or $n = 1$, corresponding to the typical neutron star of $M \sim 1.4M_\odot$ and $R \sim 10$ km. We have numerically calculated the subsequent evolution from these initial conditions. We ignored the dissipative viscosity terms for internal motions during the evolution of the orbit, so that the stellar circulation is conserved before tidal torque is important. We will give our results of numerical simulations below.

3.1 Tidal distortion

We show the typical examples of the quadrupole deformation of stars with $n = 0.5$ and $n = 1$ in Fig.1. The initial state corresponds to $\chi = 0$, but the results are almost the same for $\chi \neq 0$. Three orthogonal principal axes, a_1 , a_2 and a_3 , of the ellipsoid are shown as a function of the orbital separation. The minimum separation distance corresponds to the contact of the binary. That is, $r \sim 2.4R$ for $n = 0.5$ and $r \sim 2.3R$ for $n = 1$. The axes a_1 and a_2 are located on the orbital plane, while a_3 is the direction of the orbital angular momentum. The a_1 -axis is initially chosen as the separation direction \mathbf{n} of the binary, but the direction does not exactly follow the orbital motion during the dynamical evolution. The orbital revolution at small r becomes so fast that the principal axis slightly deviates from the direction \mathbf{n} , i.e., there is a time lag. We will discuss the lag angle in next subsection. However, the lag angle is small, so that the star is elongated almost in the separation direction \mathbf{n} and compressed in other two directions. The quadrupole deformation becomes significant for $r < 5R$ and grows as $|a_i/R - 1| \propto r^{-3}$. The internal structure also affects the shape of the ellipsoids. The model with $n = 1$ is more centrally condensed than that with $n = 0.5$, so that the shape is less deformed. The difference is, however, a few percent in the magnitude. We will see how this difference appears in the orbital motion and gravitational radiation below.

3.2 Orbital motions

The binary evolution driven by the gravitational radiation is calculated in terms of four approximations to estimate various forces. (1) All post²-Newtonian, spin and tidal effects are included. (2) The post²-Newtonian effects are included, but the stars are regarded as point masses. (3) Purely Newtonian gravity is used, but the tidal effects are included. (4) The Newtonian gravity is used, and the stars are regarded as point masses. We show the angular and radial velocities in Fig.2 and Fig.3. We give the comparison between the approximations (1) and (2) in Fig.2a and Fig.3a, and the comparison between the approximations (3) and (4) in Fig.2b and Fig.3b. The difference due to the approximations becomes clear below $r \sim 3R$, where the star is much deformed. The model with $n = 0.5$ is more deformed and therefore the deviation from the point mass approximation becomes more significant. Although the spin-orbit force with positive χ are repulsive, the post-Newtonian corrections, spin-spin and tidal force are dominant attractive forces. Combined with all these effects, the final approaching velocity significantly accelerates.

The absolute magnitude of the velocity shifts, when the post-Newtonian corrections are included. The ratio, i.e., the direction of colliding stars, may be more useful than the absolute values as the initial conditions of the hydrodynamical simulation after the coalescence. We show the velocity ratio $-V_r/V_\phi$ in Fig.4. The approaching velocity increases up to ten percent of the orbital angular velocity, i.e., the velocity ratio $-V_r/V_\phi \sim 0.1$ at the contact of the binary. This ratio further increases with decrease of the polytropic index n , because the tidal force is larger.

When the binary separation is large enough, the binary evolves at much longer time-scale compared with that of the internal motions. The stellar figure is tidally locked at this stage. As the time-scale of the orbital motion decreases, the tidal lock becomes loose and the lag angle becomes non-zero. We show the lag angles for two stellar models ($n = 1$ and $n = 0.5$) in Fig.5. The negative lag angles means that the elliptical figure does not follow the orbital revolution, and that there is a time lag to settle down. The lag angles amount to 0.1 radian just before the contact. This suggests that both stars at the coalescence touch each other not in the longest axis of the ellipsoid, but the direction slightly deviates.

3.3 Gravitational wave forms

The tidal force affects the orbital motion just before the contact. We have synchronized the phase of the gravitational wave at the initial separation $r = 15R$. In Fig.6 and Fig.7, we only show the evolution of the gravitational wave forms radiated at the last several revolutions. The correction of tidal force in the amplitude is of order $I/(\mu r^2) \sim \beta \varepsilon^2$. Therefore, tidal effect is a small correction in the amplitude, but it accumulates in the phase of the wave. As the time proceeds, the wave form deviates from that of point masses, which is represented by the dotted line in Fig.6. The deviation of the $n = 0.5$ model is larger than that of the $n = 1$ model, because of larger tidal deformation. The phase shift becomes significant only for the last a few revolutions, and the amount of the phase shift is less than π , if there is no initial spin. In Fig.7, we show the dependence of the initial spin. The stellar spin gives large difference in the phase shift. For the larger initial spin, the repulsive spin-orbit force becomes stronger, so that it takes much longer time to contact each other. The amount of the phase lag becomes more than π for the fast spinning case.

3.4 Evolution of spin

The stellar spin is modified through the tidal torque following eq.(17). We have calculated the evolution of the spin from various initial states. We show the typical evolution of the spin in Fig.8. The variations of spins are quite small at large separation, but monotonically grow only in the final stage, $r < 4R$. The stars significantly deviate from the spherical state as mentioned in §3.1, and the tidal torque becomes quite large there. Therefore, variation of the spin is quite a steep function of r , since the tidal torque is $dJ/dt \propto I r^{-3} \propto r^{-6}$. We also show the total amount of the change of the spin for the

various initial spin angular momentum in Fig.9. The transferred momentum through the tidal torque decreases with the increase of the parameter χ . The angular momentum is much more transferred in the counter-rotating star with the orbital angular momentum, i.e, star with negative χ .

4 Discussion

The simple estimate of the tidal effect is of order $\sim \beta\epsilon^2 f_N \sim \epsilon^5 f_N$, as shown in §2.1. The final state of the binary corresponds to $\epsilon \sim 0.3$, so that the correction seems to be $(0.3)^5 \sim 0.002$, but is much large in the actual problem. The discrepancy comes from the existence of the marginal circular radius, where the hydrodynamical instability occurs [12]. If the radiation reaction force is not included, there are circular orbits for any separations, but they are not always stable [23]. We expect that there exists innermost stable circular orbit, which the post-Newtonian gravity and the tidal force cause at the critical separation. Two stars significantly accelerate in the radial direction below this critical radius. In a future paper, we will show that the location of the innermost stable circular orbit is affected by polytropic index n and initial spin parameter χ . The tidal effects at the last a few cycles cause large radial infall velocity, lag angle and spin-up. The higher post-Newtonian corrections or fully relativistic hydrodynamical calculation will be required to study much more correct final phase. The topic treated in this paper is preliminary, but will be useful as the guide for the future theoretical work and the observations by the advanced type of the laser interferometer.

Acknowledgment

This work was supported in part by the Japanese Grant-in-Aid for Scientific Research of the Ministry of Education, Science and Culture (No.05218208, 06740225).

References

- [1] A. Abramovici et al., *Science* **256**, 325 (1992).
- [2] R. Narayan, T. Piran & A. Shemi, *ApJ*. **379**, L17 (1991).
- [3] E. S. Phinney, *ApJ*. **380**, L17 (1991).
- [4] B. F. Schutz, *Nature* **323**, 310 (1986).
- [5] C. Cutler et al., *Phys.Rev.Lett.* **70**, 2984 (1993).
- [6] W. Lincoln & C. Will, *Phys.Rev.D* **42**, 1123 (1990).
- [7] L. Blanchet et al., *Phys.Rev.Lett.* **74**, 3515 (1995).
- [8] H. Tagoshi & T. Nakamura, *Phys.Rev.D* **49**, 4016 (1994).
- [9] H. Tagoshi & M. Sasaki, *Prog.Theor.Phys.* **92**, 745 (1994).
- [10] X. Zhuge et al., *Phys.Rev.D* **50**, 6247 (1994).
- [11] T. Nakamura, in: "*Relativistic Cosmology*", eds M. Sasaki, Universal Academy Press, Inc.-Tokyo, Japan (1994), p.155.
- [12] D. Lai, F. A. Rasio & S. L. Shapiro, *ApJ*. **420**, 811 (1994).
- [13] D. Lai, F. A. Rasio & S. L. Shapiro, *ApJ*. **423**, 344 (1994).
- [14] D. Lai, F. A. Rasio & S. L. Shapiro, *ApJ*. **443**, 705 (1995).
- [15] T. Damour & G. Schäfer, *IL NUOVO CIMENTO* **101B**, 127 (1988).
- [16] J. B. Hartle, K. S. Thorne & R. H. Price, in: "*Black Holes: The Membrane Paradigm*", eds K. S. Thorne et al., Yale University Press, New Haven and London, USA. (1986), Chap.V.
- [17] B. Carter & J. P. Luminet, *MNRAS*. **212**, 23 (1985).
- [18] J. P. Luminet & B. Carter, *ApJS*. **61**, 219 (1986).
- [19] S. Chandrasekhar, "*Ellipsoidal Figures of Equilibrium*", Yale University Press, New Haven, in USA. (1969).
- [20] G. Schäfer, *ANNALS OF PHYSICS* **161**, 81 (1985).
- [21] K. D. Kokkotas & G. Schäfer, *MNRAS* **275**, 301 (1995).
- [22] C. S. Kochanek, *ApJ*. **398**, 234 (1992).
- [23] L. E. Kidder et al., *Phys.Rev.* **D47**, 3281 (1993).

Figure Captions

Fig.1a: Variations of the tri-axes of ellipsoid with $n = 0.5$ and $\chi = 0$ as a function of the binary separation. The solid, dashed, and dotted lines indicate the axis a_1 , a_2 , and a_3 .

Fig.1b: The same as Fig.1a, but with $n = 1$.

Fig.2a: The angular velocity at the binary separation r . The solid line denotes the result included post²-Newtonian, spin-orbit, spin-spin and tidal forces with $n = 0.5$ stellar model without initial spin. The dashed line is the same but with $n = 1$ model. For comparison, the result of point mass, neglecting the tidal and spin effects, is described by the dotted line.

Fig.2b: The same as Fig.2a, but the results are based on the purely Newtonian calculation. The solid and dashed line denote the results included tidal forces with $n = 0.5$ and $n = 1$ models, respectively. The dotted line is the result of point mass.

Fig.3a: The radial velocity of the binary with relativistic corrections. The meaning of each line is the same as in Fig.2a.

Fig.3b: The radial velocity of the binary with Newtonian gravity. The meaning of each line is the same as in Fig.2b.

Fig.4a: The velocity ratio $-V_r/V_\phi$ in the coalescing binary with relativistic corrections. The meaning of each line is the same as in Fig.2a.

Fig.4b: The velocity ratio $-V_r/V_\phi$ in the coalescing binary with Newtonian gravity. The meaning of each line is the same as in Fig.2b.

Fig.5: The lag angle for the binary without the initial spin. The solid and dashed lines correspond to $n = 0.5$ and $n = 1$, respectively.

Fig.6a: The gravitational wave forms h_+ from the binary with polytropic index n . The solid and dashed lines correspond to the result of $n = 0.5$ and that of $n = 1$, respectively. Result of point masses is also given by the dotted line for comparison.

Fig.6b: The same as Fig.6a, but for the gravitational wave forms h_\times .

Fig.7a: The gravitational wave forms h_+ of the binary with $n = 0.5$ from various initial spin states. The solid, dotted and dashed lines correspond to $\chi = 0, 1, 2$.

Fig.7b: The same as Fig.7a, but the initial spin is counter-rotating. The solid, dotted and dashed lines correspond to $\chi = 0, -1, -2$.

Fig.8: Variation of stellar spin with all corrections. The solid line represents the evolu-

tion for $n = 0.5$ model, and the dashed line for $n = 1$. The initial spin is zero.

Fig.9: Total change of the spin angular momentum for various initial χ values. The filled circles and triangles correspond to $n = 0.5$ and $n = 1$ model.

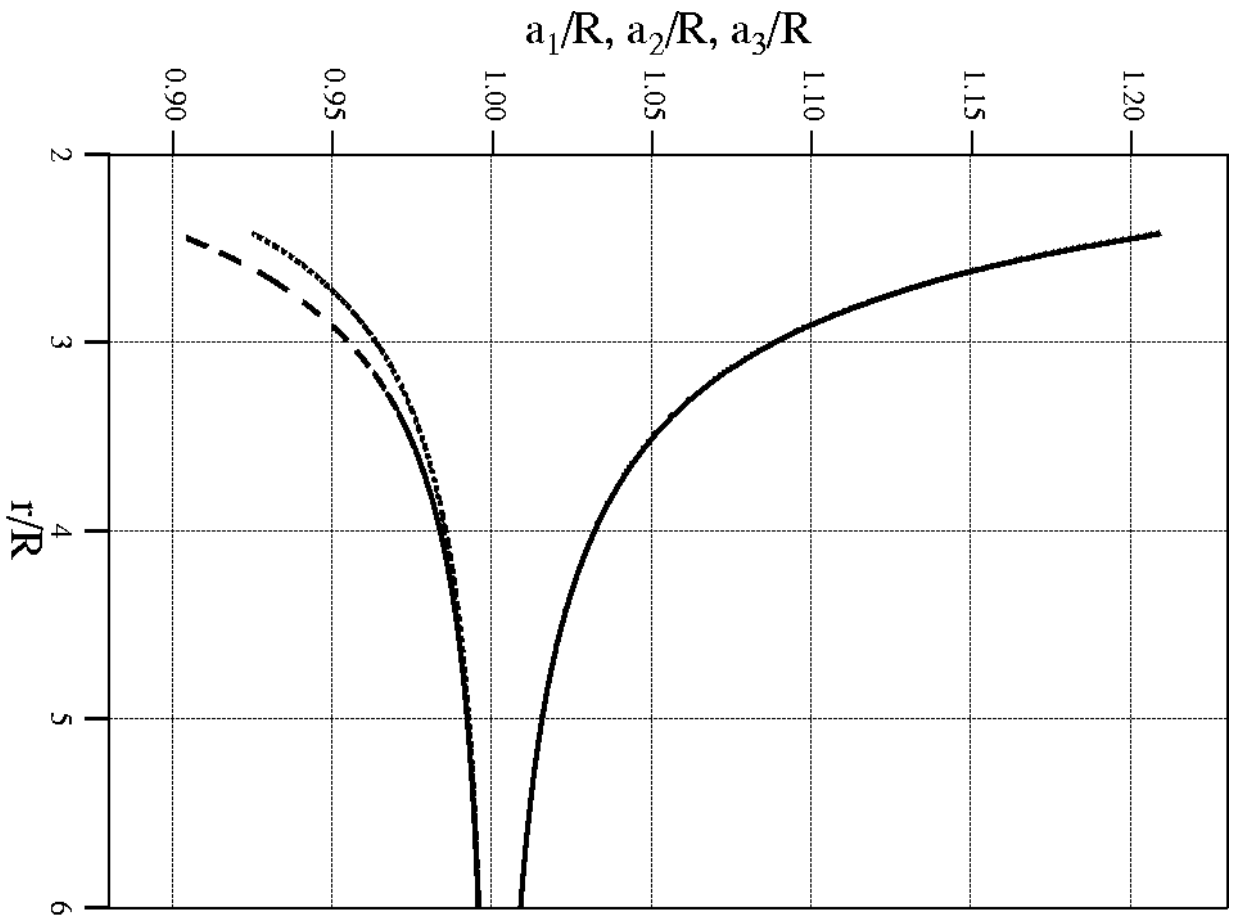


Fig. 1a

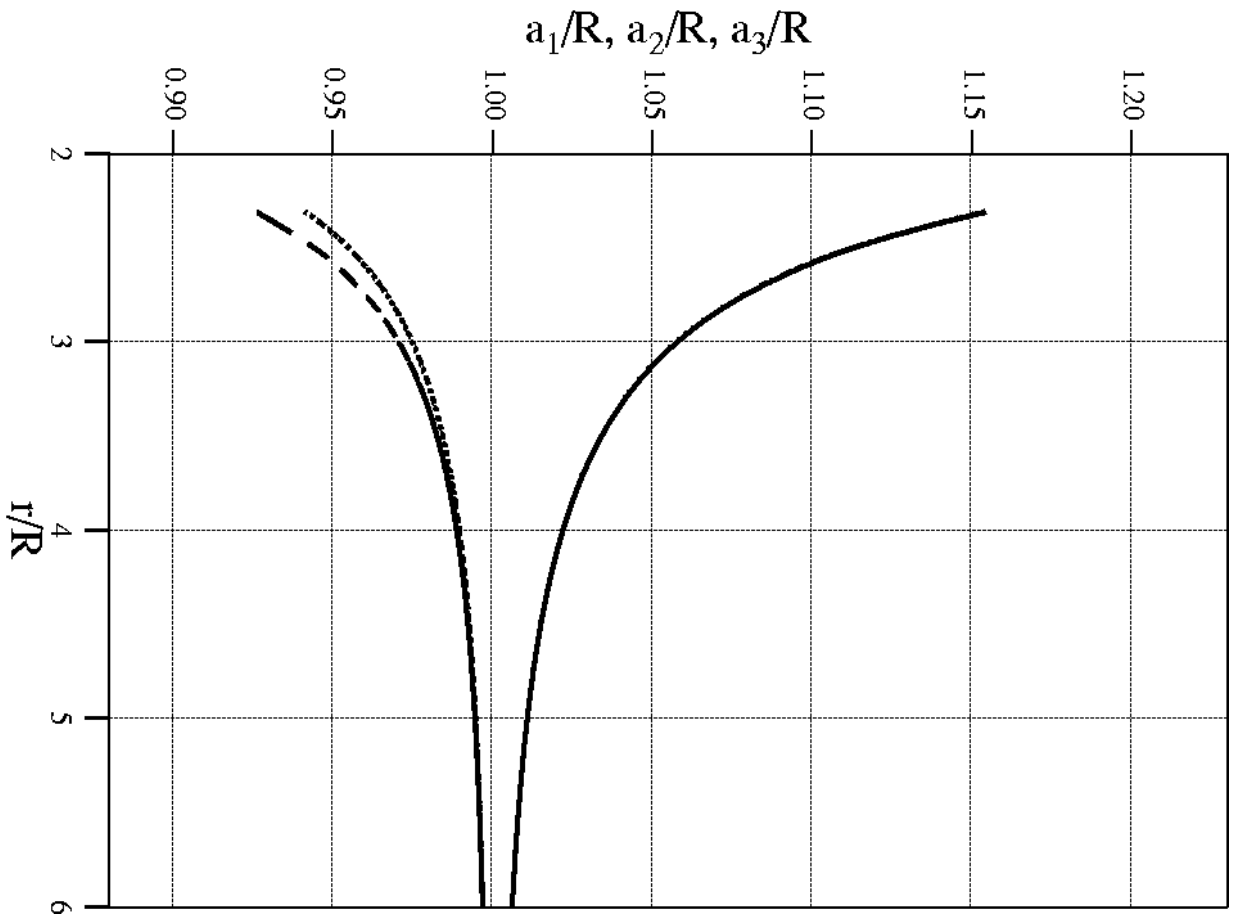


Fig. 1b

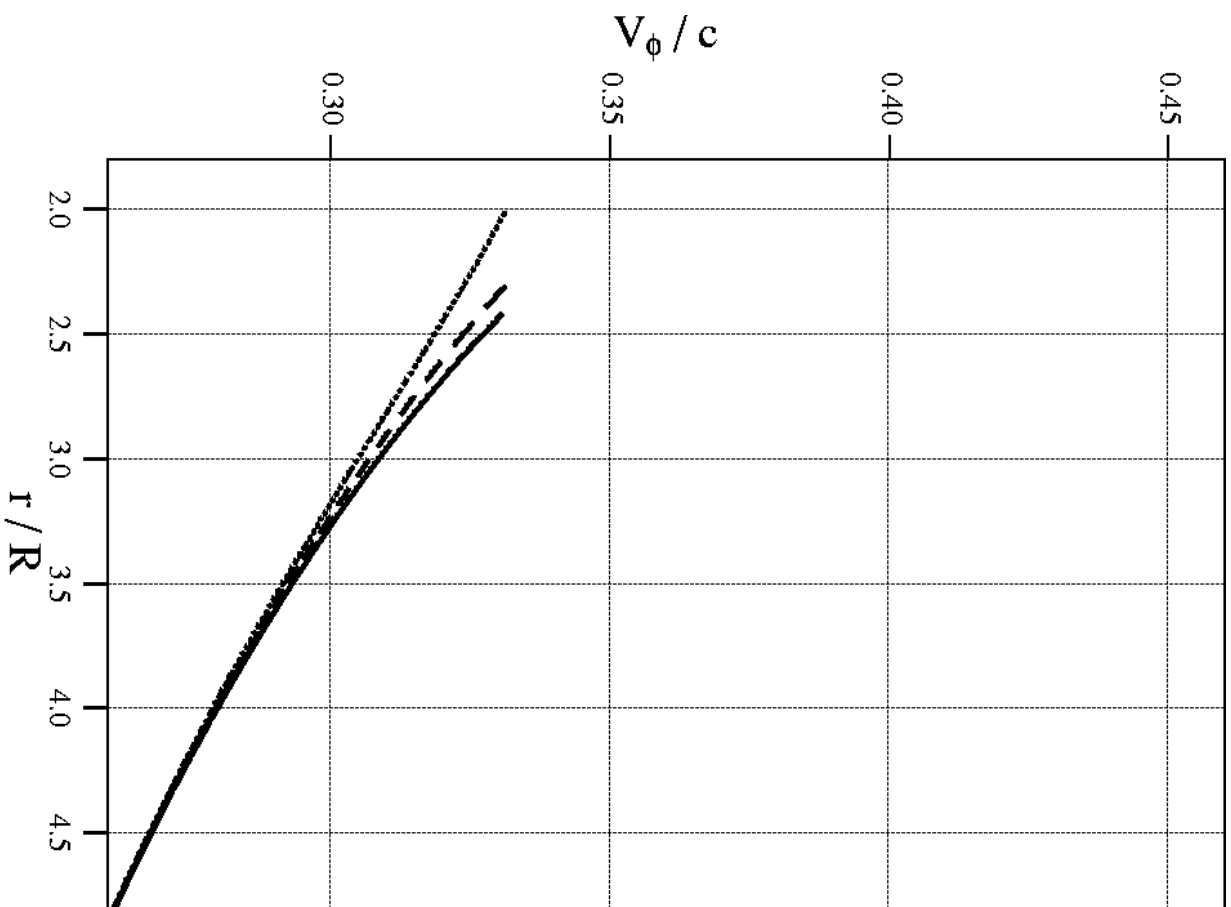


Fig.2a

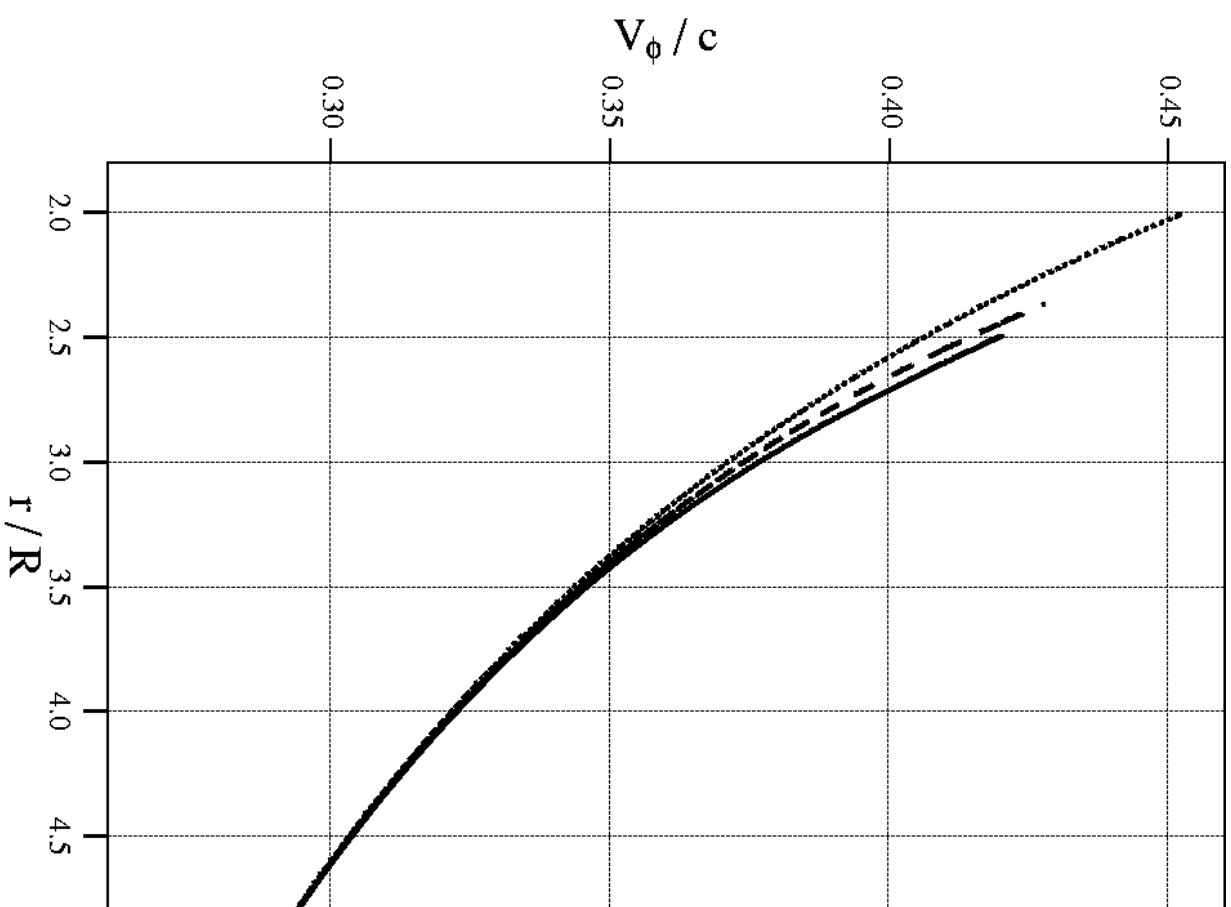


Fig.2b

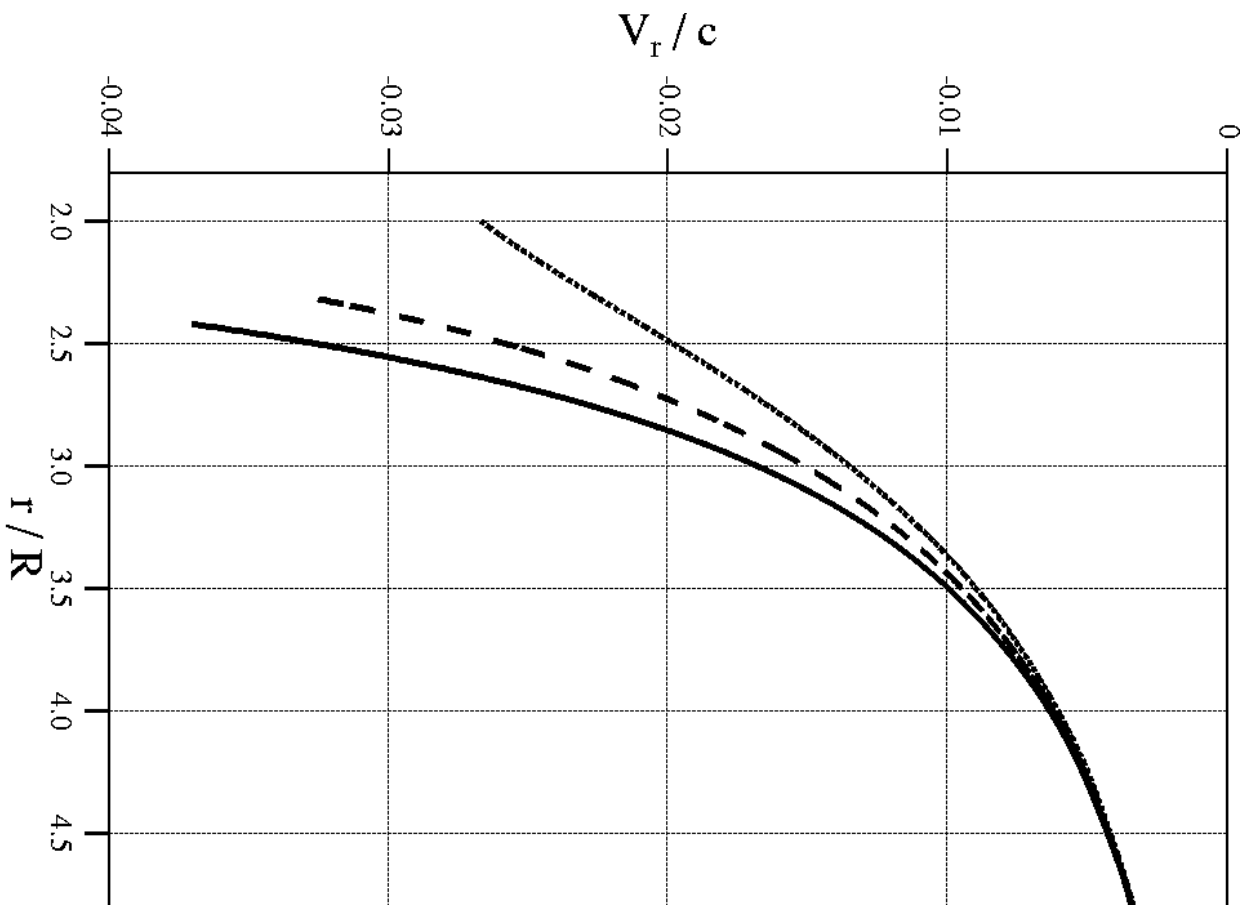


Fig.3a

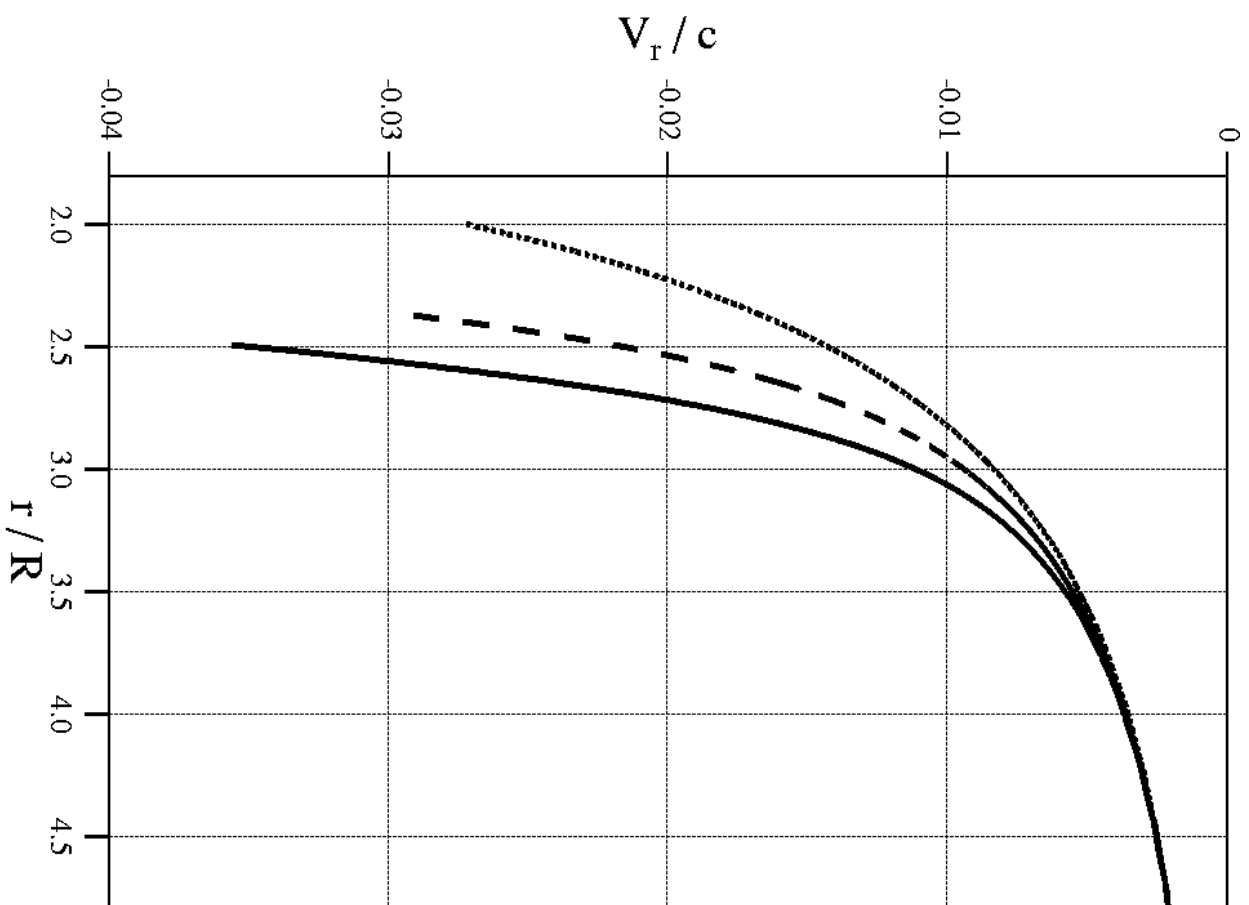


Fig.3b

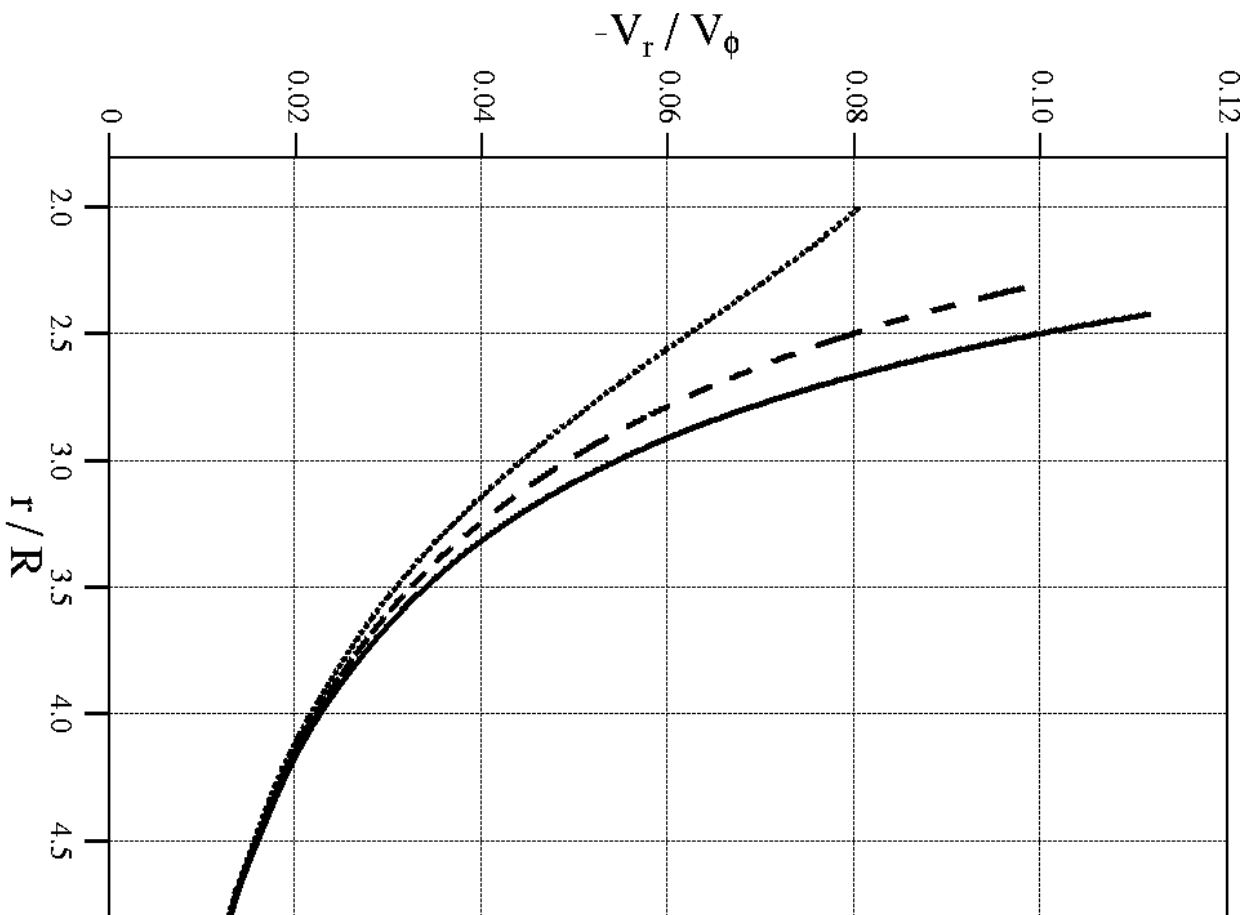


Fig.4a

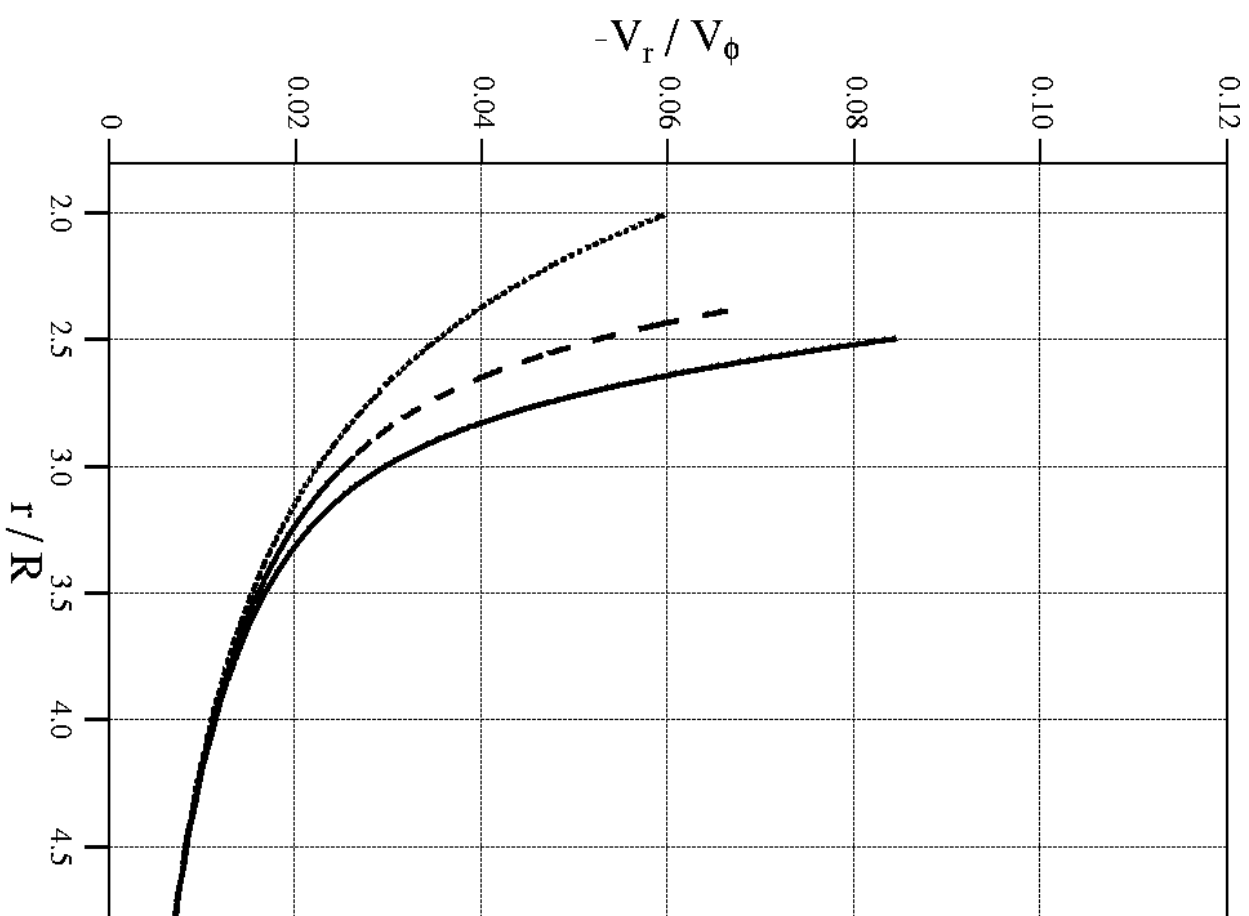


Fig.4b

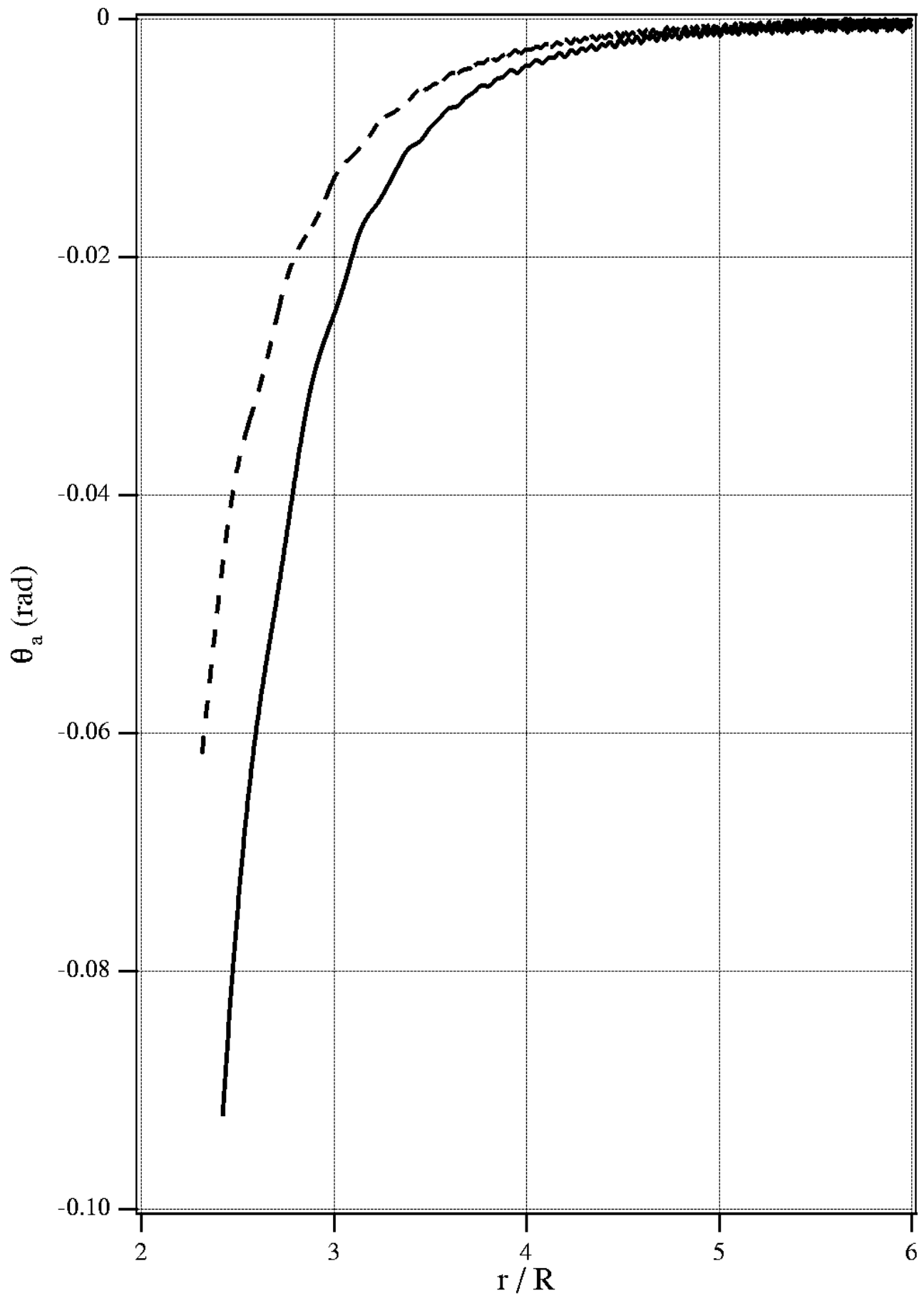


Fig.5

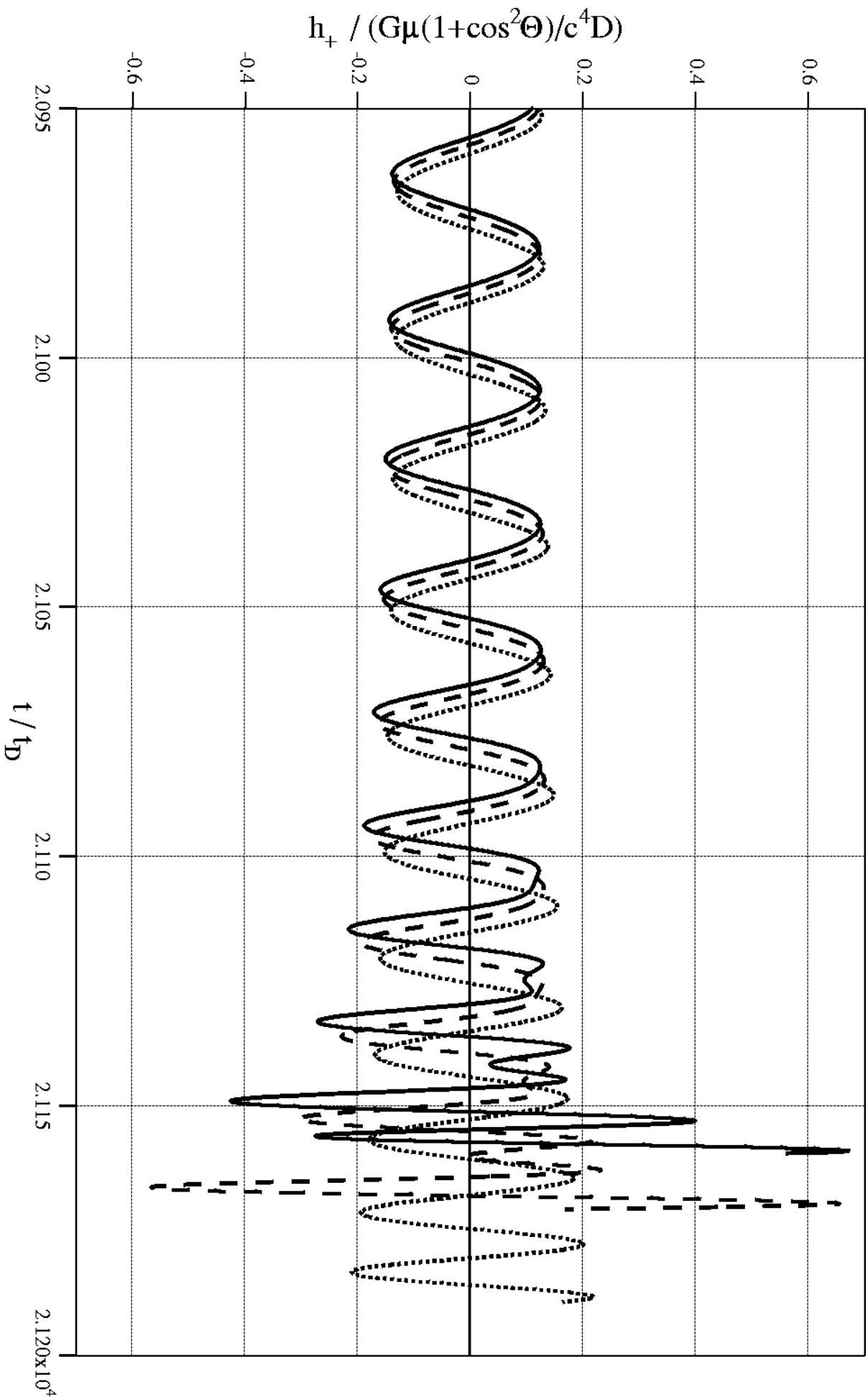


Fig.6a

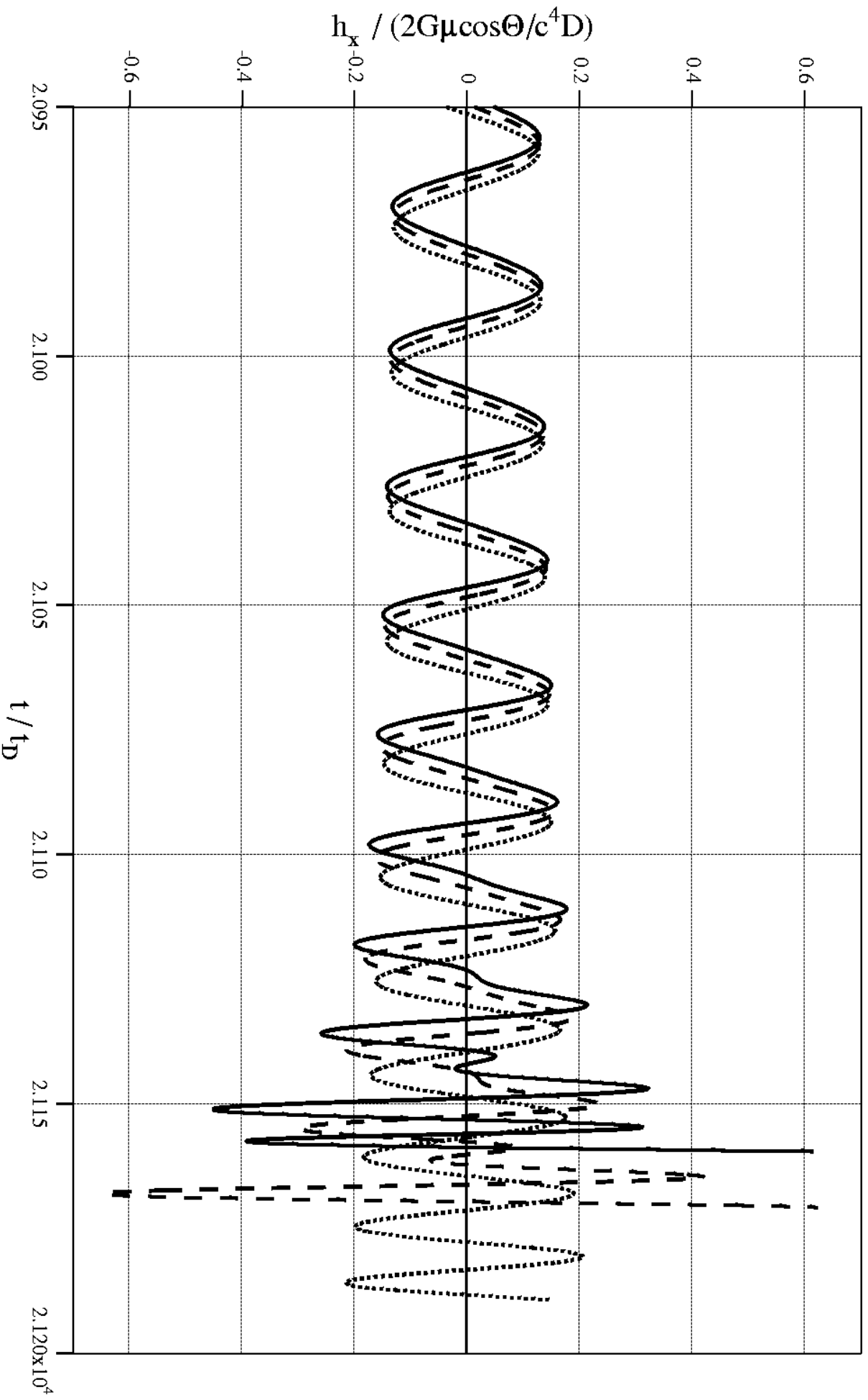


Fig.6b

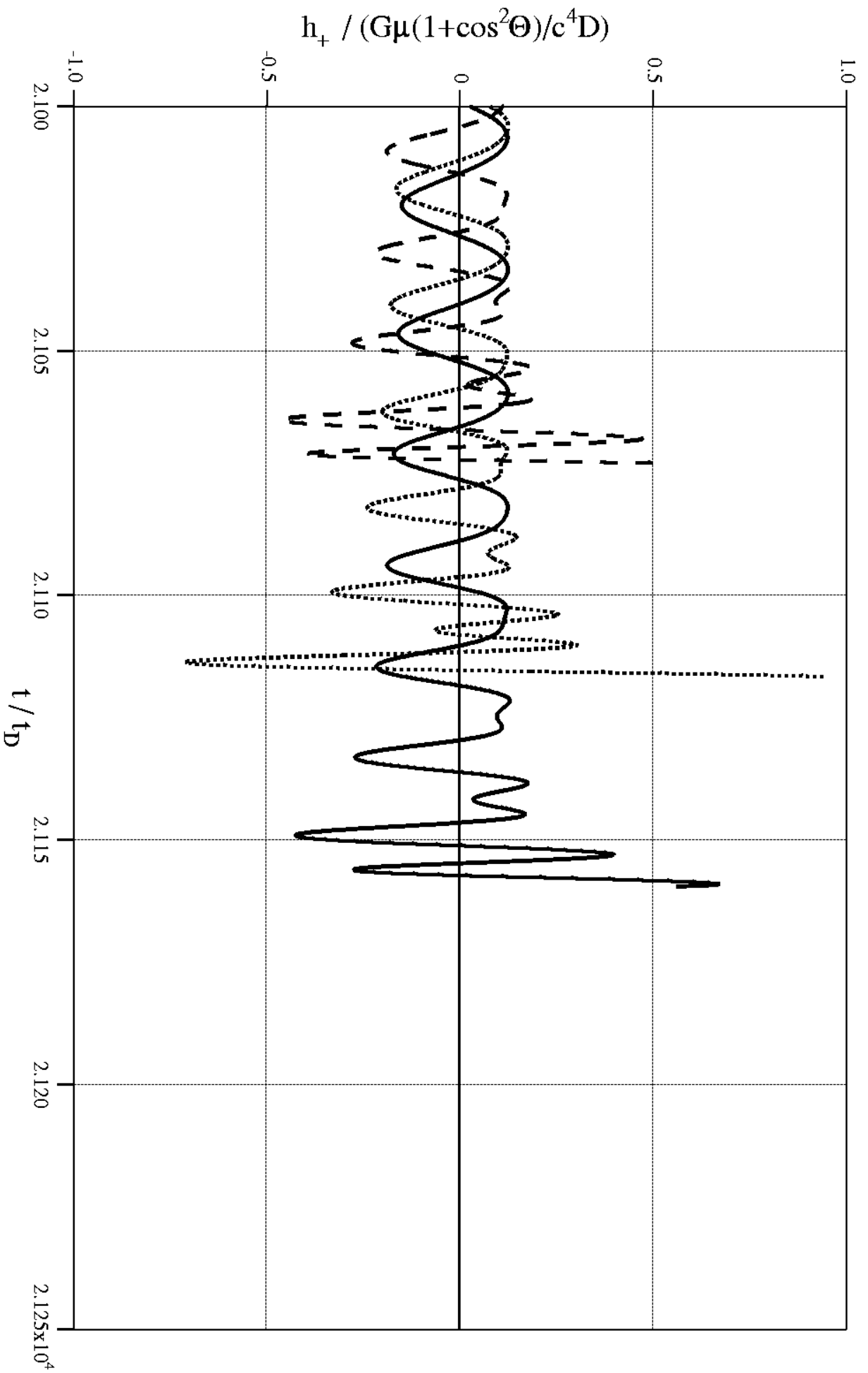


Fig. 7a

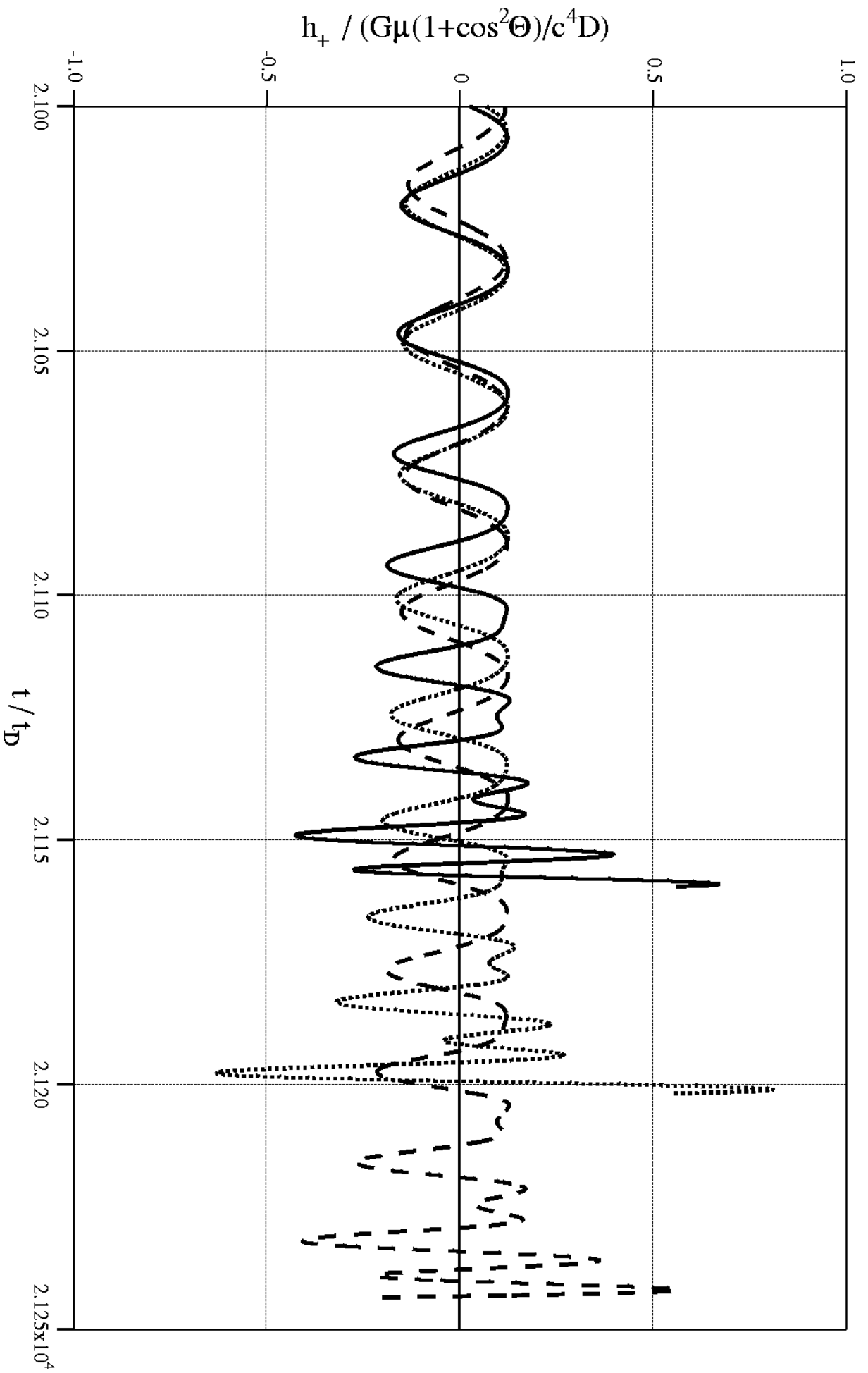


Fig. 7b

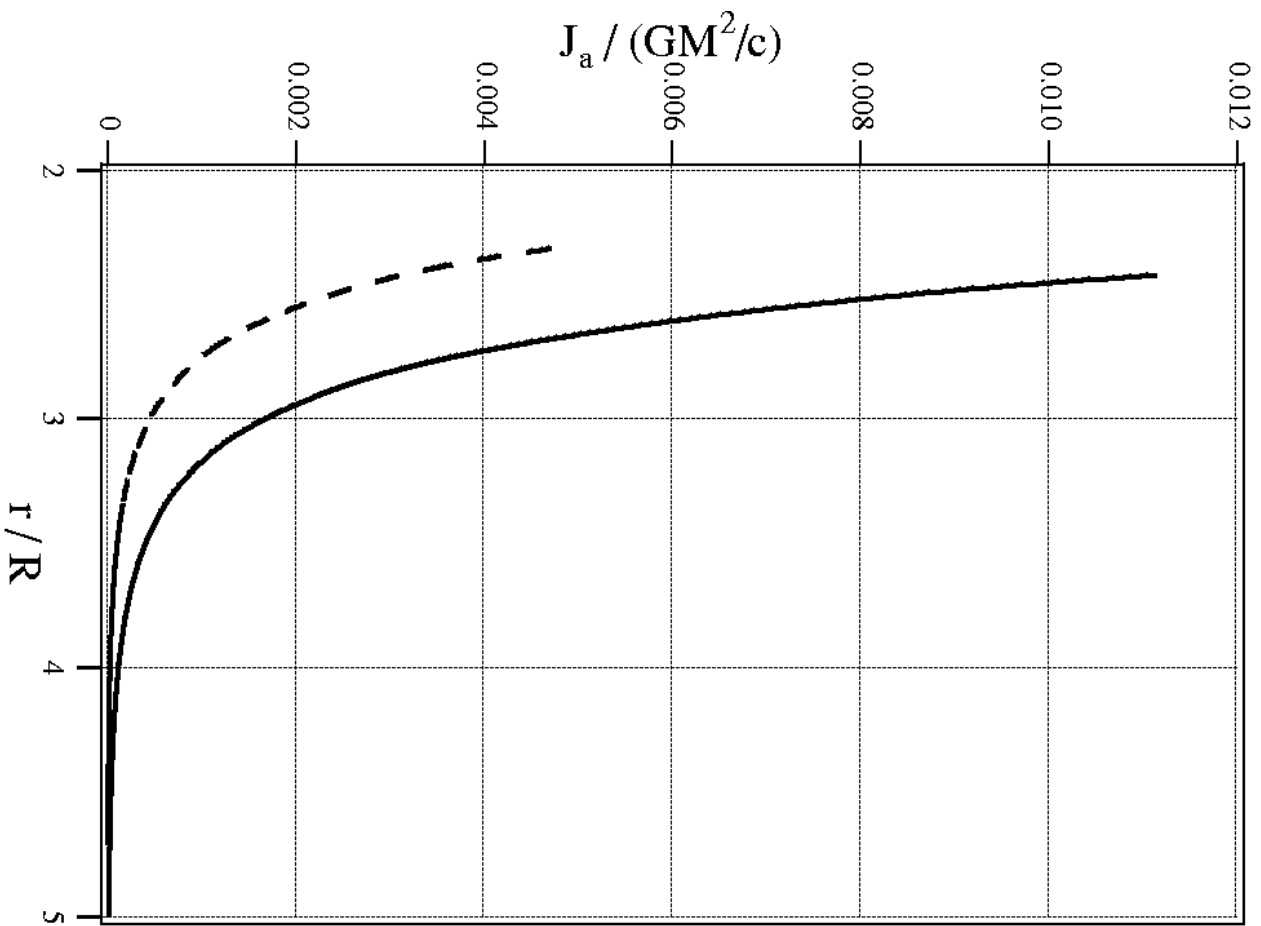


Fig.8

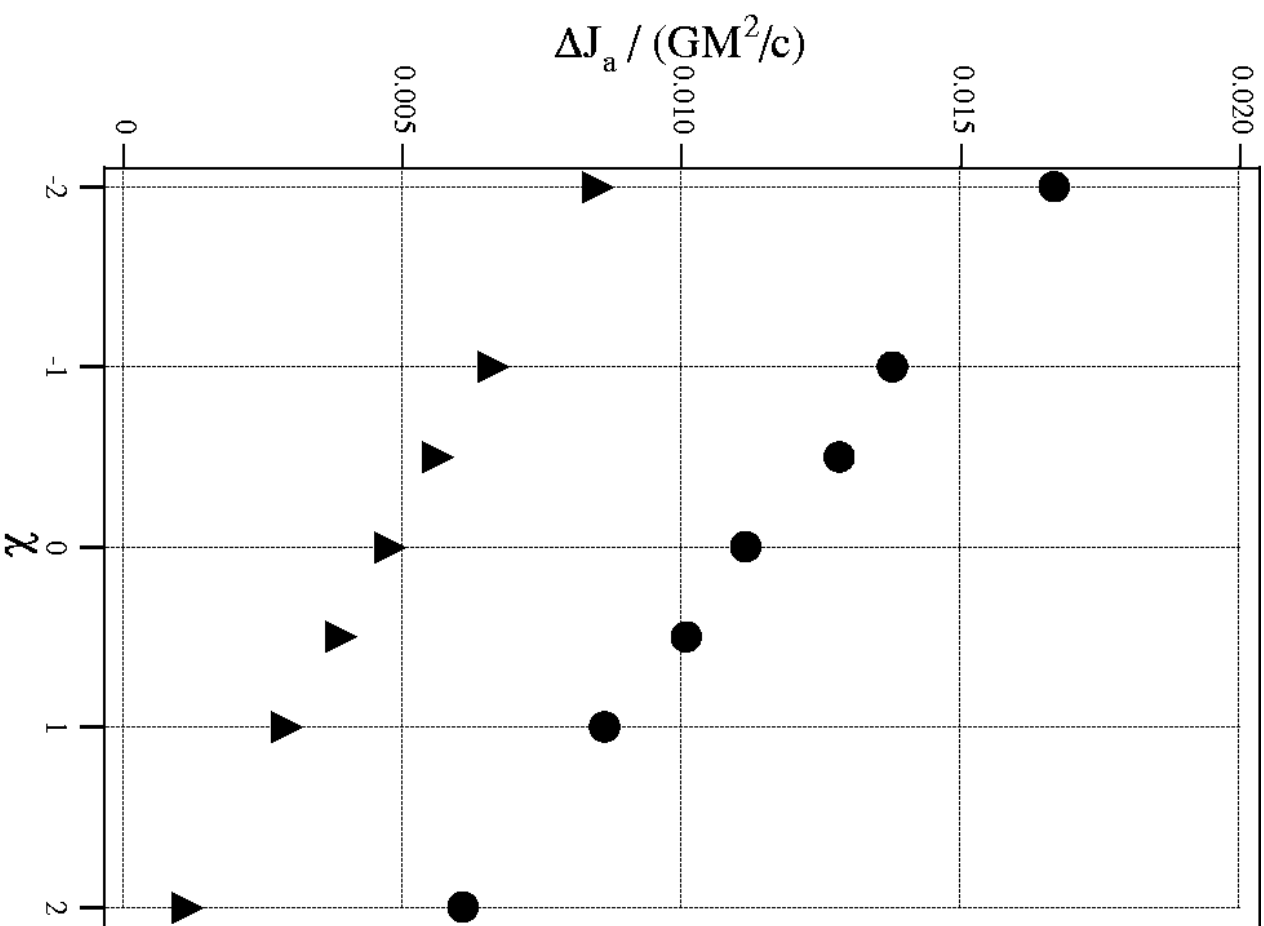


Fig.9